EFFICIENT TOPOGRAPHIC CORRECTIONS FOR RESISTIVITY DATA①

He, Jishan

Central South University of Technology, Changsha 410083, China

ABSTRACT

The development of topography effect correction on resistivity data was summed up. Mainly the correction technique based on angular domain superposition and ratio method was discussed to solve point source and 2–D topography problem. The nature of ratio topography correction was proved and the results were spread to point source. Based on systematically studying anomalies of angular domains with different angles, a fast method of topography correction was presented which can be run on personal computer and get resonable accuracy

Key words: topographic correction angular domain cubic spline

1 INTRODUCTION

Resistivity methods are widely used in the search of mineral resources, groundwater and geothermal, and in engineering applications, but topography may affect the resistivity data seriously. Study of topographic effects in resistivity surveys may be divided into three phases. Before the 1960's, it was done basically with scale modeling[1]. In 1970's 2–D calculation methods were developed[2–4]. Later, correction methods for 2–D terrain with a point source, using an angular domain as a basic terrain element, were developed by the author *et al*[5~8] and further numerial modeling was studied in China[9–11]. In the mentime Fox *et al* systematically studied topographic effects in resistivity and I P surveys based on finite element numerical modeling[12].

Besides scale modeling we can divide the way of solving terrain with point source problem into two classes. The first is based on numerical modeling, it can be used to simulate topography / ore body anomaly caused by both topography and structures; the other is based on angular domain superposition. It can be employed only to compute the topographic effect of a point source on 2–D terrain surface.

2 THE FACTORS OF TERRAIN EFFECT IN RESISTIVITY SURVEY

Topography affects on resistivity survey seriously. It causes spurious anomalies when the earth is homogeneous. The terrain not only produces anomalies but also distorts the anomalies due to inhomogeneity when ore bodies / structures exist. Our problem is how to remove the topographic anomalies or how to distinguish anomalies due to underground bodies from intensive background of topographic

①Manuscript received March 15, 1992

effects.

To guantitatively analyze the effects of topography on resistivity survey, we discuss the case shown in Fig. 1. Suppose that the earth is homogeneous and its resistivity is ρ_o. Because of the rising and falling of the ground surface, what we measured is apparent resistvity ρ_a

$$\rho_a = k(\triangle U / I)$$

where K is geometric factor; $\triangle U$ is the electric potential difference between the potential electrodes p_1 and p_2; I is the current supplied into the earth through current electrodes. When the space between p_1 and p_2 is small we get

$\triangle U = El = \triangle x / \cos\alpha = \rho_o j_{12} \triangle x / \cos\alpha$ where E is electric field intensity of p_1 and p_2; $\triangle x$ the horizotal distance between p_1 and p_2; l the distance between p_1 and p_2; j the current density of p_1 and p_2. Therefore, we have

$$\rho_a = (K\triangle x / I)\rho_o \ j_{12} / \cos\alpha)$$

Because $I / (K\triangle x)$ is the current density of p_1 and p_2 when the surface of homogeneous earth is flat, it can be written as j_o. So we have

$$\rho_a = (\rho_o / j_o)(j_{12} / \cos\alpha) \qquad (1)$$

This expression can illustrate the anomaly due to topography in principle. It shows that the topographic effects on resistivity survey is very complex. The terrain makes the distance between electrodes different from that on flat earth, the more important thing is that it changes electric field distribution.

3 ANGULAR DOMAIN IS THE BASIC 2–D TERRAIN ELEMENT

The ridge, valley and slope are often taken as basic topographic elements. We did in the same way originally. However, after further study on the features of topographic resistivity anomalies, we found that whenever there is a change of slope of the ground surface there will be a topographic anomaly. So we decided that angular domain is the basic 2–D terrain element. As shown in Fig. 2, angular domain is the area within two infinite crossing planes. The medium resistivity of angular domain is homogeneous and isotropic.

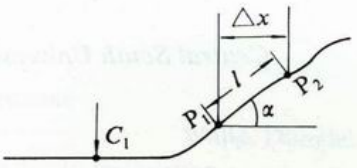

Fig. 1 A scheme for analysing resistivity anomaly

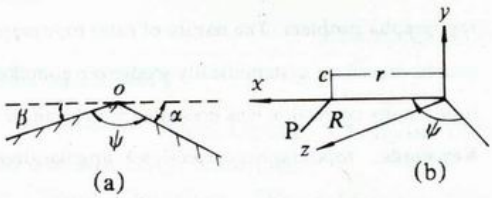

Fig. 2 A scheme of 2–D angular domain topography

The cylindrical coordinate system (r,θ, z) is selected so that the z axis coincides with the strike of the angular domain and the two slopes coincide with planes of $\theta=0$ and $\theta=\psi$, respectively. Put current source G at position $(r_c,0,0)$ and P, at which to calculate the electric potential, at $(r_P, 0, z)$. Separation of variables is used to solve Laplace's equation. The electric potential U_P at point P can be obtained as follows[7]:

$$U_P = \frac{2\rho_o I}{\pi^3}\int_o^\infty \cos(tz)\int_o^\infty \frac{\mathrm{sh}(s\pi)\mathrm{ch}[s(\psi-\theta)]}{\mathrm{sh}[s(\psi)]} \times K_{is}(t,\gamma_c)K_{is}(t,\gamma_p)\mathrm{d}s\mathrm{d}t \qquad (2)$$

Where $K_{is}(t,\gamma_c)$ and $K_{is}(t,\gamma_p)$ are functions of the third kind of Bessel's. After a series of transformations, expression (2) can be rewritten as a series for convenience of calculation.

$$U_p = \frac{\rho_o I}{\pi\psi\sqrt{\gamma_c \cdot \gamma_p}}\{\frac{1}{2}Q_{-\frac{1}{2}}(\xi) + \sum_{m=1}^{\infty}\cos\frac{m\theta\pi}{\psi}Q_{\frac{m\pi}{\psi}-\frac{1}{2}}(\xi)\} \qquad (3)$$

where $\xi = |(r_c^2 + r_p^2 + Z^2)/(2r_c r_p)|$ (4)

$Q_\gamma(\xi)$ is a functrion of the second kind of Legendre's. When γ is an integer, the following recurrence formula can be used.

$$\left.\begin{aligned} &Q_0(\xi) = \ln[(\xi+1)/(\xi-1)]/2 \\ &Q_1(\xi) = \xi Q_o(\xi) - 1 \\ &\cdots\cdots \\ &Q_n(\xi) = [(2n-1)\xi/n \\ &Q_{n-1}(\xi) - (n-1)Q_{n-2}(\xi)] \end{aligned}\right\} \quad (5)$$

The following formula is for non-integral γ:

$$Q_\gamma(\xi) = \Gamma(\gamma+1)\Gamma(\frac{1}{2})/(2\xi)^{\gamma+1}\Gamma(\gamma+\frac{3}{2}) \times F(\frac{\gamma+1}{2}, \frac{\gamma+2}{2}, \gamma+\frac{3}{2}, \frac{1}{\xi^2}) \quad (6)$$

where $\Gamma(x)$ is the gamma function and F is hypergeometric function with series form

$$F(\alpha,\beta,\gamma,\chi) = 1 + \frac{\alpha\cdot\beta}{\gamma\cdot 1}\chi + \frac{\alpha(\alpha+1)\beta(\beta+1)}{\gamma(\gamma+1)\cdot 1\cdot 2}\chi^2 + \cdots\cdots, (x<1) \quad (7)$$

Katsuro Maeda obtained expression (3)[8]. However, the problem was not completely solved because there were still singular points. All the given curves in his paper did not run over the vertex points of dipping bebs.

$Q_\gamma(\xi)$ has a logarithmic singular point when $\xi = 1$. In this case, $Z = 0$ and $r_p = -r_c$, current source C and measurement point p are at the symmetric points of two angular domain flanks. However they are not singular points in a physical sense, so other kinds of expression must be used for this case. After a series of transformations on expression (4) and paying attention to $z = 0$ and $r_p = -r_c$, we obtain

$$U_p = \frac{\rho_o I}{\pi\psi\gamma_c}\{\frac{\pi}{4} + \sum_{m=1}^{\infty}(-1)^m \times [\psi(m+\frac{1}{2}) - \psi(\frac{m\pi}{\psi}+\frac{1}{2})]\} \quad (8)$$

where

$$\psi(x) = \lim_{n\to\infty}[\ln^n(-\frac{1}{x} - \frac{1}{x+1} - \frac{1}{x+2} \cdots - \frac{1}{x+n}] \quad (9)$$

When the current electrode lies at the vertex point of an angular domain, the current density is π/ψ of that in homogeneous half space, so the electric potential at point P is

$$U_p = \rho_o I/2\psi\sqrt{r_p^2 + z^2} \quad (10)$$

According to the principle of reciprocity, the potential when P is at vertex point of angular domaim is

$$U_p = \rho_o I/2\psi\sqrt{r_c^2 + z^2} \quad (11)$$

Using expressions (3), (8), (10) and (11), the electric potential of any point of the angular domain can be calculated completely. To test those expressions, we made systematic calculations on angular domains with various values of ψ, α and β, and compared with simulation experiments with a large water tank. The comparison shows that our formulas are correct. Fig. 3 is an example of an angular domain of $\psi = 60(^\circ)$. The resuts of calculation using the expressions above and the results of simulating experiments fit each other very well. It is an extreme case. People can not do any electric survey on a slope of $60(^\circ)$ but it is a good testing case for its large terrain anomaly. In addition the very interesting phenomenon is that ρ_a has negative values on the right side of the top, due to the special distribution of electric field.

4 FORM 2–D TOPOGRAPHY WITH ANGULAR DOMAIN SUPERPOSITION

A 2–D topography of rolling hills and valleys as shown in the cross section of Fig. 4 can be simplified with broken lines. Each pair of adjoining lines forms an angle. Because the

lengths of these broken lines are limited, they are not the angular domains. However, we can imagine that they are more and more close to angular domain with increase of the length. So we take each pair of adjoining lines as an angular domain. The vertex angles of angular domains in Fig. 4 are ψ_1, ψ_2, ···. The topographic anomaly measured at certain point of a continuously rising and falling topography is a function of anomalies of corresponding angular domains, that is

$$\frac{\rho_a}{\rho_o} = F[(\frac{\rho_a}{\rho_o})_1, (\frac{\rho_a}{\rho_o})_2, \cdots, (\frac{\rho_a}{\rho_o})] \qquad (12)$$

where $(\rho_a / \rho_o)_1$, $(\rho_a / \rho_o)_2$, ···, $(\rho_a / \rho_o)_n$ are anomalies of each angular domain at corresponding points. Because the topographic anomalies of each angular domain can be obtained from expressions above, we can calculate the anomalies of any 2–D topography, if we get the function or relation F. By a large number of comparisons of calculated and experimental results, we found that the anomaly of a continuous topography can be obtained multiplicative superposition of anomalies.

$$\frac{\rho_a}{\rho_o} = (\frac{\rho_a}{\rho_o})_1 (\frac{\rho_a}{\rho_o})_2 \frac{1}{\cos\beta^2} \cdots\cdots (\frac{\rho_a}{\rho_o})_n \frac{1}{\cos\beta_n} \qquad (13)$$

where β_2, ···β_n are the slope angles of angular domains at that point.

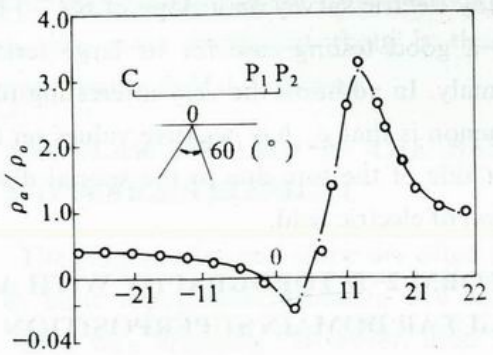

Fig. 3 Comparision between calculation circle and scale modeling curve of 3–electrode array profile on a 60(°) angular domain.

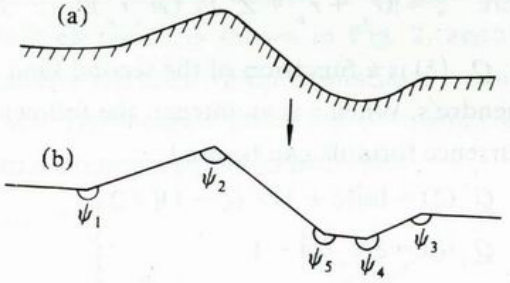

Fig. 4 Using 2–D topography formed by broken lines (b) to replace 2–D topography (a) of rolling hills and vallys

To test the approximate extent of formula (13), we made many superposition calculations and compared them with scale modeling results of various ridges, valleys and slopes with various arrays and different electrode spaces. The results show that the average relative deviation between scale modeling and numerical superposition is less than 4% for ridge or valley if the slope is less than 30(°). Therefore, it is acceptable to calculate 2–D topographic anomalies with expression (13).

5 RATIO METHOD OF TERRAIN–CORRECTION FOR APPARENT RESISTIVITY DATA

The following empirical formula called "Ratio Method" terrain correction, has been used in China to correct the terrain effects of apparent resistivity for many years:

$$\rho_c = \rho_a / (\rho_t / \rho_o) \qquad (14)$$

where ρ_c is apparent resistivity corrected; ρ_a is apparent resistivity measured; ρ_t / ρ_o is nomalized apparent resistivity anomaly of topography

Though it is an empirical method, it can reduce the topographic effects in large degree and distinguish anomalies due to the structure.

To find out the regularity of the changes of apparent resistivity after ratio correction, let

us to study the simple case of a 2–D problem including sources topography and structure. The plane $z(x, y)$ in Fig. 5 is normal to the strike of the 2–D surface indicated with SR, C is current source with line form,

P_1 and P_2 are two potential electrodes. Because it is 2–D problem, conformal mapping can be used. Plane $z(x, y)$ is mapped onto plane $w(u, v)$ so that the surface, $R'S'$ on the plane w becomes flat. But after they are mapped into plane w, the distance between adjacent stations, is not constant, e.g. $12 = 1'\ 2'$.

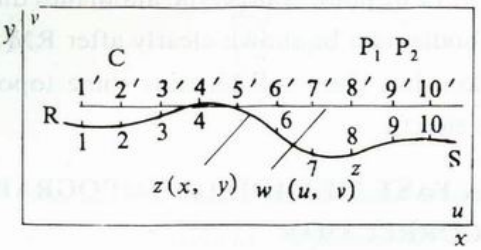

Fig. 5 A Scheme of 2–D source and topography, conformd mapping plane $z(x, y)$ onto $w(u, v)$

Because of assuming homogeneous earth the apparent resistivity anomaly, expressing with ρ_t, on plane z is due to irregular surface and

$$\rho_t = K_Z(\triangle U / I) \tag{15}$$

where $K_z = \pi / \ln|CP_1| / |CP_2|$ is the geometric factor of plane z.

On plane w, because the earth is homogeneous and flat, the measured apparent resistivity is the actual resistivity.

$$\rho_0 = K_w(\triangle U' / I) \tag{16}$$

where $K_W = \pi / \ln(|C'\ P_1'| / |C'\ P_2'|)$ is the geometric factor of plane w. Pay attention to $\triangle U = \triangle U'$, then we have

$$\rho_t / \rho_0 = K_Z / K_W \tag{17}$$

The result above is very interesting. It tells that the ratio of apparent resistivity anomaly caused by terrain effect to the resistivity of the medium just equals to the ratio of geometric factors of plane z to those of plane w. Fig. 6 is a set of 2–D simulating results . The dotted lines are topographic anomaly curves. The small circles show the value of K_z / K_w. This two fit each other very well. So expression(17) is proved.

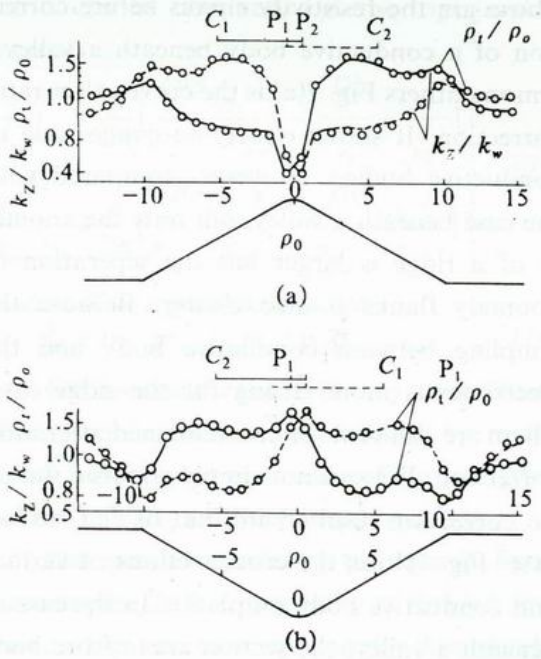

Fig. 6 Comparison between ρ_t / ρ_0 and K_z / K_w

From plane z to w, the irregular surface becomes flat and the electrode spaces become various from station to station. Before ratio method correction, the geometric factor is calculated with electrode space as a constant in plane z. So the terrain anomaly arise.

The apparent resistivity measured along the surface on plane z is

$$\rho_a = K_z(U / I) \tag{18}$$

After ratio correction on it

$$\rho_c = \rho_a / (\rho_t / \rho_0) \tag{19}$$

Therefore, for 2–D problem , the ratio correction for terrain effects is actually to map stations from plane z to w, then calculate geometric factors of plane w.

Can this way completely remove terrain

effects from apparent resistivity of field data? If the earth is homogeneous, this will do; Otherwise the ratio correction results can not remove terrain effects completely but simply reduce it and make the anomalies clear.

Fig. 7 shows a set of modeling results. Those are the resistivity curves before correction of a conductive body beneath a valley . Among others Fig. 7(a) is the curves after ratio correction. It shows clearly anomalies due to conductive bodies. However, compared with the case beneath a valley, not only the anomaly of a ridge is larger but the seperation of anomaly flanks is also clearer. Because the coupling between conductive body and the electrodes is more strong for the ridge case. There are still some effects remained after ratio correction. We can not simply equalize the ratio correction results with that of flat surface case; Fig. 7(b) is the cross sections of surface and conductive body on plan z. In the case of beneath a valley, the section area of ore body becomes larger, and the electrode spacings over the ore body increased. To do the measurements on plane z with different station spacings and draw the curves on plane z, as shown in Fig. 7(a) , we will find that it is the same as the curves after ratio corrected. The similar results will occur in the case of a ridge, but after mapping plane z onto w, the section area of the ore body, beneath the ridge, will be decreased, the top depth shortened, and the station spacings decreased. The measurement results on plan w are also the same as the results of corrected, see Fig. 7(c).

The case of point source field is more complicated than the case of line source. It is impossible to find out the simple formulas like expressions (17) and (19) in point source case. However, by large number of modelings, theory calculations and field survey results, we can get following conclusions:

(1) The topographic anomalies of point and line sources have the similar shapes, but the anomaly of point source is greater than that of line source. The differnce between the anomalies of these two sources depends on the spacing between electrodes, and it is greater when the spacing is small. In addition the anomalies due to point source and line source close to each other when electrodes spacing is larger than terrain size;

(2) For point source, the anomalies due to ore bodies can be shown clearly after RM correction, but there still remains some topographic effects.

6 A FAST METHOD OF TOPOGRAPHY CORRECTION

The key to topographic correction of apparent resistivity using the ratio method(RM) is to obtain the apparent resistivity anomaly caused by topography only. The topography anomaly of angular domain topography can be calculated by analytic expressions. In fact , we developed a series of programs according to eguations (3)~ (14), which have been used successfully in the resistivity data processing. However, the expressions include multiple infinite series, which make the computing time too long especially around singular points. A method of calculating electrical potential distortion with cubic spline function, hence the obtaining topographic anomaly is discussed here. With it , topographic anomalies can be calculated by superposing any limited angular domain elements formed by the angular domain elements of any angles between 90(°) ridge and 270(°) valley domain. In addition computer program has been developed, with

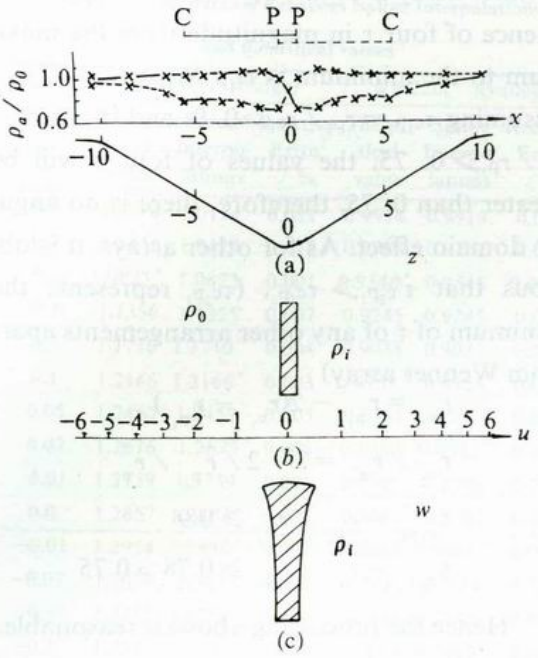

Fig. 7 Scale modeling results to show the nature of ratio correction for 2−D problem.

line(solid and doted)—data measured on plane z along the valley and after ratio correction; x—data measured on plane w along flat surface with various station spacing

which topographic anomalies and the corrected apparent resistivity can be obtained quickly.

6.1 *Pricinple of the method*

To emphasize the topographic effect, we nomalize equation (3) by

$$U_0 = \rho_0 I / 2\pi |r_c - r_p|$$

Then we obtain

$$D(\psi,\tau) = 2|1-\tau| \{Q_{-\frac{1}{2}}(\xi) + \sum_{m=1}^{\infty} (\tau/t)^m \times Q_{\frac{m\pi}{\psi}-\frac{1}{2}}(\xi)\} / \psi\sqrt{t} \quad (20)$$

$$\tau = \begin{cases} r_c / r_p, & |r_p| > |r_c| \\ r_p / r_c, & |r_c| > |r_p| \end{cases} \quad (21)$$

$$t = |\tau| \quad (22)$$

where r_c and r_p are the separations between coordinate origin and C, P respectively. D is the electric potential distortion of angular domain. Function $D(\psi, \tau)$ is a curved surface.

From equation(20) , the potential distortion of topography with arbitrary apical angle ψ and arbitrary electrode separation can be calculated, hence topographic anomalies of all points can be obtained, *e.g.* the topographic anomaly is

$$\left.\begin{aligned} (\frac{\rho_a}{\rho_0})_{c_1} &= \frac{K}{2\pi}[\frac{D(\tau_{c_1p_1})}{|r_{c_1} - r_{p_1}|} - \frac{D(\tau_{c_1p_2})}{|r_{c_1} - r_{p_2}|}] \\ (\frac{\rho_a}{\rho_0})_{c_2} &= \frac{K}{2\pi}[\frac{D(\tau_{c_2p_2})}{|r_{c_2} - r_{p_2}|} - \frac{D(\tau_{c_2p_1})}{|r_{c_2} - r_{p_1}|}] \end{aligned}\right\} \quad (23)$$

where K is a geometric factor

$$K = 2\pi c_1 p_1 \cdot c_1 p_2 / p_1 p_2 \quad (24)$$

The anomaly caused by any two dimensional topogrphy can be obtained by multiplying topographic anomalies of every angular domain at every station by equation (13).

The specific calculating techique is, first , the complex 2−D topography is divided into the combination of many angular domain elements, for each angular domain element, from the value of the apex ψ, the relevant D, potential distortion, for each variable τ can be obtained by interpolation; second, the topographic anomaly of each domain is calculated from equation(23) and then the topographic anomaly of the combined topography is obtined from equation(13) .

6.2 *Processing in the Computing Program*

(1) In the computing program the potential distortion and derivative, 331 values in total, have been stored in memory corresponding to ψ = 90, 100, 110, 130, 150, 170, 190, 210, 230, 250, 270 and the relevant τ = 0.9, 0.7, 0.5, 0.3, 0.2, 0.1, 0.05, 0.02, 0.01, 0.00, −0.01, −0.02, −0.05, −0.1, −0.2, −0.3, −0.4, −0.5, −0.7, −0.9, −1.0, All these potential distortions

are obtained from formula (20) . We take these potential distortions as the values of interpolating base point τ. If the calculated angular domain apex is exactly one of the ψ values stored above, we can directly use each τ value relevant to this ψ as interpolating base point and do interpolation in ψ direction. Otherwise, we do interpolation in the direction first to get the values of base point corresponding to ψ, then do interpolation in the ψ direction. The average error between the results of two times interpolation is $<0.2\%$.

(2) If both of the current electrode and potential electrode are at the same side of the angular–domain apex and far from the apex, the effect of the angular domain is negligible, only the effect of slope will be considered. To save time, there is an automatic processing in the program that if the four electrode arrangement is used , four τ will be calculated at each station, and if one of them is greater than 0. 9, it will be considered that the relevant potential distortion anomalies of four τ are nonexistent, hence the other three τ will not be calculated. The accuracy of this technique will be proved as follows.

From theoretical calculations, the angular domain effect is nagligible if the ratio of r_{cp}, (the distance between current point C and potential point P) to r_c, (the distance between curent applying point C and angular domain apex) is less than 1 / 3, that is, $r_{cp} / r_c < 1 / 3$, hence

$$\tau = \frac{r_c}{r_p} = \frac{r_c}{r_c + r_{cp}} \geqslant 0.75 \qquad (25)$$

that is , if $\tau \geqslant 0.75$, the angular–domain effect can be neglected.

As show in Fig. 6, r_{c_1}, r_{c_2}, r_{p_1} and r_{p_2} are distances from c_1, c_2, p_1 and p_2 to apex 0. As far as the worst condition is considered , if the Wenner array is used, $r_{c_1p_1} = r_{p_1p_1} = r_{p_2c_2}$, the sequence of four τ in magnitude from the maximum to the minimum is $\tau_{c_1p_1}$, $\tau_{c_1p_2}$, $\tau_{c_2p_2}$, $\tau_{c_2p_1}$, . Assuming $\tau_{c_1p_1} = r_{p_1} / r_{c_1} \geqslant 0.9$, and if $\tau_{c_2p_2} = r_{c_2} / r_{p_1} \geqslant 0.75$, the values of four τ will be greater than 0. 75, therefore, there is no angular domain effect. As for other arrays, it is obvious that $\tau'_{c_2p_1} \geqslant \tau_{c_2p_1}$, ($\tau_{c_2p_1}$ represents the minimum of τ of any other arrangements apart from Wenner array) .

$$\because \quad r_{c_2} = r_{p_1} - 2(r_{c_1} - r_{p_1})$$

$$\therefore \quad r_{c_2} / r_{p_2} = 3 - 2 / r_{p_1} / r_{c_1}$$

$$\because \quad \tau_{c_1p_1} = r_{p_1} / r_{c_1} \geqslant 0.9$$

$$\therefore \quad \tau_{c_2p_1} = r_{c_2} / r_{p_1} \geqslant 0.78 > 0.75$$

Hence the processing above is reasonable.

6. 3 *Calculations and Examples*

(1) Table 1 gives the potential distortions at $\psi = 140(^\circ)$ and $\psi = 220(^\circ)$, their relevant analytical values by cubic spline interpolating function, and their relevant errors. The table shows that the precision of the interpolation is high, the maximum relative error is 0.021% but the relative errors are generally less than 0.009% and the average relative errors of both are 0. 007% and 0. 005% respectively;

(2) To examine the precision of calculations for individual angular–domain, the calculations of topography anomalies for many sets of individual angular domains are compared. For the ridge topography of $\psi = 90(^\circ)$, the theoretical values are obtained by mirror image analysis. Both calculations are shown in Fig. 8, which shows that the calculations have high precision. Comparing calculations by mirror image with those of interpolation, the average error of differential field array is 0.100 %, and that of electrical sounding is 0.098%.

(3) Fig. 9 shows an example of the

Table.1 Comparison Betweens Spline Interpolations and theoritical values

τ	$\psi=140(^\circ)$(ridge)			$\psi=220(^\circ)$(valley)		
	Theoritical value	Spline Interpolations	Relative Error / %	Theoritical value	Spline Interpolations	Relative Error / %
0.9	1.0116	1.0114	0.021	0.9916	0.9916	0.001
0.7	1.0431	1.0429	0.018	0.9760	0.9762	0.004
0.5	1.0823*	1.0823	0.001	0.9546*	0.9546	0.0025
0.3	1.1356	1.1355	0.007	0.9245	0.9245	0.003
0.2	1.1710	1.1710*	0.004	0.9038	0.9037	0.007
0.1	1.2166	1.2166*	0.003	0.8753*	0.8753	0.002
0.05	1.2460	1.2459	0.005	0.8551	0.8551*	0.000
0.02	1.2676	1.2675	0.008	0.8382	0.8382*	0.003
0.01	1.2759	1.2759	0.001	0.8305	0.8306	0.007
0.0	1.2857	1.2857*	0.002	0.8181	0.8182	0.007
−0.01	1.2954	1.2954*	0.002	0.8061	0.8061*	0.003
−0.02	1.3038	1.3037	0.006	0.7990	0.7988	0.022
−0.05	1.3252	1.3252*	0.003	0.7845	0.7845*	0.005
−0.1	1.3537	1.3536	0.006	0.7693	0.7693*	0.003
−0.2	1.3947	1.3947*	0.002	0.7518	0.7518*	0.001
−0.3	1.4223	1.4222	0.006	0.7419	0.7419*	0.003
−0.4	1.4412	1.4411	0.009	0.7358	0.7358*	0.006
−0.5	1.4540	1.4539	0.006	0.7319	0.7319*	0.002
−0.7	1.4682	1.4681	0.006	0.7278	0.7278	0.006
−0.9	1.4727	1.4724	0.019	0.7264	0.7263	0.016
−1.0	1.4742	1.4741	0.007	0.7260	0.7260*	0.005
Average relative error			0.007			0.005

* ——Rounding off number.

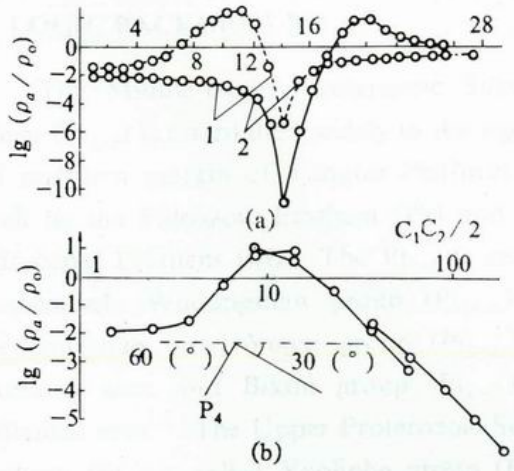

Fig. 8 Resistivity anomalies due to a ridge with $\psi=90(^\circ)$

1——mirror image analysis; 2——cubic spline interpolation results; (a)——electrode differential array; (b)——Schlumberger sunding at point P.

copmarison of scale modeling with cubic spline function interpolations by statistics, we obtained the maximum relative error is 3. 4%, the average relative error is 1. 04%;

(4) From theoretical studies, experiments and field data processing, it has been proved that the topography correction by cubic spline inter-polating function fully meets the precision requirment of the field practice and has the advantages of fastness and easiness, and it can give all results in one time for various topographies.

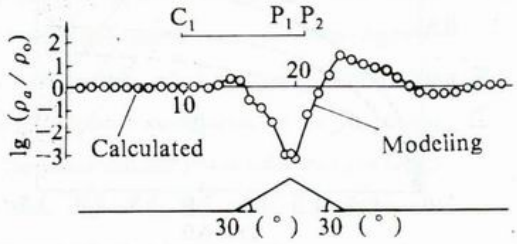

Fig. 9 Comparison of scale modeling with cubic splining function interpolations

The fast correction method above is for 2–D structures, point sources and profiles normal to strike. We can use expressions(3) ~ (11) and (13) or some additional coeffcients if the profile is oblique to the strike. Strictly speaking, the topography is of three dimensions. It is very difficult to calculate apparent resistivity of a 3–D topography with any shape. To deteramine the differences between 2–D and 3–D topography, a lot of scale modeling has been done. First, we use scale models with different cross sections and very long strike so that they are essentially 2–D topographies. Measurements were made along the central profile which is at the strike center and normal to the strike. Then we shortened the strike from two ends symmetrically and made measurements still along central profile. The results are summarized as follows:

1) If the cross sections are the same, 3–D and 2–D topographies have similar charactristics and the anomalous amplitude of 3–D is larger than that of 2–D;

2) The anomaly of a valley is smaller than the one of a ridge if their cross sections are mirror images each other;

3) With increaing strike, a 3–D topography approximates a 2–D one. Fig. 10 is a summary of modeling results. From it we can say that in most cases, we can consider an actual topography as a 2–D if its length is larger than array length. So the method above can be used very widely.

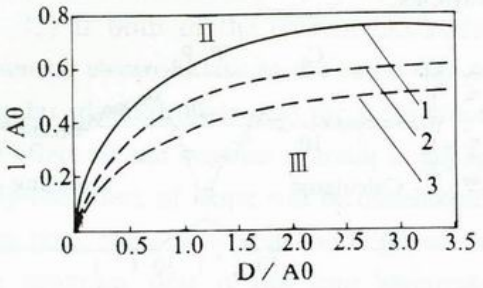

Fig. 10 The transition from 3–D to 2–D

1—triangle section with slope of 20~ 30(°); 2—paraboloid section; 3— isoscales trapezoid section; II — the range of 2–D; III—the range of 3–D

REFERENCES

1 Chantulishvele, L. S. Electrical Prospecting for Road Design in Varied Topographic Regions, Moscow; 1965.

2 He, Jishan *et al.* Science and Technique of Mining and Metallurgy, 1976, (3).

3 Ge, Weizhong. Acta Geophysiga Sinica, 1977, 20 (4).

4 He, Jishan. Geology and Exploration, 1975, (8); 45–51.

5 He, Jishan. Journal of Gentral South Institute of Mining and Metallurgy. 1978,(2).

6 He, Jishan *et al.* The Interpretation of DG Electrical Methods, Changsha: GSIMM press, 1978.

7 He, Jishan *et al.* Electrical Prospecting for Metalliferous Deposits. Beijing; Metallurgical Industry Press, 1980.

8 Maeda, Katsuro. Geophysics, 1955, 20(1); 123–139.

9 Li, Daqian *et al.* The Application of Finite Element Method in Electrical Well Logging. Beijing; Petroleum Industrial Publishing House, 1980.

10 Zhou, Xixiang *et al.* Computing Technique of Geophysical and Geochemical Prospecting, 1980,(2) .

11 Zhou, Xixiang *et el.* Acat Geophysica Sinica 1983, 26(3).

12 Fox, R. C. *et al.* Geophysics, 1980, 45(1); 75–93.